

Detecting Planets around Low-mass Stars in the Kepler Field

Clement Gaillard

A senior thesis submitted to the faculty of  
Brigham Young University  
in partial fulfillment of the requirements for the degree of  
Bachelor of Science

Dr. Denise C. Stephens, Advisor

Department of Physics and Astronomy

Brigham Young University

December 2015

Copyright © 2015 Clement Gaillard

All Rights Reserved

## ABSTRACT

### Detecting Planets around Low-mass Stars in the Kepler Field

Clement Gaillard

Department of Physics and Astronomy, BYU

Bachelor of Science

As the Kepler space telescope searched for transiting Earth-like planets, it observed thousands of stars, including a large collection of M-dwarfs. M-dwarfs are stars that are smaller, cooler and fainter than our Sun. Finding transiting planets around an M-dwarf is difficult because of the low signal-to-noise observations made by the Kepler mission for these specific stars. Using PyKE, a Python-based package developed by the NASA Kepler Guest Observer Office, we can minimize the noise introduced by the star and its neighbors to produce cleaner light curves for the fainter M-dwarfs. With this package we were able to produce light curves for 113 M-dwarfs in the Kepler database. We analyzed this data and detected transiting planet candidates. We present our methodology and analysis for one transiting planet candidate that we discovered.

Keywords: exoplanet, kepler, transiting planet, low-mass star

## ACKNOWLEDGMENTS

I would like to acknowledge my advisor, Dr. Denise Stephens for giving me the opportunity to work on the research project that produced this senior thesis. Without the opportunity that she gave me to go to a national meeting, I would not have met the astronomers who inspired this research project.

I would also like to acknowledge my wife Liu Yu Yu. She has always been very supportive of my passion for astronomy and exoplanets.

# Contents

<b>Table of Contents</b>	<b>iv</b>
--------------------------	-----------

<b>List of Figures</b>	<b>vi</b>
------------------------	-----------

<b>1 Introduction</b>	<b>1</b>
1.1 Exoplanets . . . . .	1
1.1.1 Definition and History . . . . .	1
1.1.2 Detecting Methods . . . . .	3
1.2 M-dwarfs Systems . . . . .	6
1.2.1 Physical Properties of M-dwarfs . . . . .	6
1.2.2 M-dwarfs Habitable Zone . . . . .	7
1.2.3 Abundance of M-dwarfs . . . . .	8
1.2.4 Abundance of Planets around M-dwarfs . . . . .	8
1.3 Kepler Space Telescope . . . . .	9
1.3.1 Mission and Purpose . . . . .	9
1.3.2 Observation Parameters . . . . .	9
1.4 Observational Challenges to Transit Detection . . . . .	10
1.4.1 Signal-to-noise Issues . . . . .	10
1.4.2 Under-sampling . . . . .	11
1.4.3 Transit Depth Limit . . . . .	11
1.4.4 Light Pollution . . . . .	11
1.5 Proposed Solution and Summary . . . . .	11
<b>2 Detection Method</b>	<b>13</b>
2.1 PSF Fitting with PyKE . . . . .	13
2.1.1 PyKE Introduction . . . . .	13
2.1.2 Field Analysis with <i>kepfield</i> . . . . .	14
2.1.3 Modeling the Field with <i>kepprf</i> . . . . .	16
2.1.4 Obtaining a New Time Series with <i>kepprfphot</i> . . . . .	20
2.2 Detrending the Time Series with KepCurve . . . . .	20
2.3 Detecting Transits with Peranso . . . . .	22
2.3.1 Period Analysis . . . . .	22

---

2.3.2	Phasing . . . . .	23
<b>3</b>	<b>Results</b>	<b>24</b>
3.1	Target Parameters . . . . .	24
3.1.1	Parameters . . . . .	24
3.1.2	Kepler's Pipeline Results . . . . .	25
3.2	Results for KepID 5080636 . . . . .	25
3.2.1	Stellar Properties . . . . .	25
3.2.2	Transit Detection . . . . .	27
3.2.3	Planet Properties . . . . .	27
3.3	Comparison and Future Work . . . . .	28
	<b>Appendix A Kepler Stellar Table</b>	<b>30</b>
	<b>Index</b>	<b>37</b>

# List of Figures

1.1	Mass-period Distribution of Discovered Exoplanets . . . . .	4
1.2	Transiting planet Effect on the Light Curve of a Star . . . . .	5
1.3	Yearly Distribution of Discovered Exoplanets . . . . .	6
1.4	Kepler’s Field of View . . . . .	10
2.1	<i>kepfield</i> Output Example . . . . .	15
2.2	PSF Model of a typical star recorded by the CCD . . . . .	16
2.3	PRF Difference Between Edge and Center of CCD Array . . . . .	17
2.4	<i>kepprf</i> Output Example . . . . .	18
2.5	<i>kepprfphot</i> Output Example . . . . .	19
2.6	Light Curve Detrended with KepCurve . . . . .	21
2.7	Merged Light Curve . . . . .	21
2.8	EEBLS Signal . . . . .	23
2.9	Phase plot for Kepler 29-b . . . . .	23
3.1	Frequency Analysis of KepID 5080636 . . . . .	26
3.2	Phased Light Curve for One Quarter . . . . .	26
3.3	Complete Phased Light Curve . . . . .	27

# List of Tables

3.1	Kepler Stellar Table Parameters . . . . .	24
3.2	KepID 5080636 Properties . . . . .	25
A.1	Kepler Stellar Table . . . . .	35
A.2	Kepler Stellar Table Parameters . . . . .	35

# Chapter 1

## Introduction

### 1.1 Exoplanets

#### 1.1.1 Definition and History

An exoplanet or extrasolar planet is a planet that orbits a star other than our Sun. Detecting exoplanets has been one of the major breakthroughs of modern astronomy, allowing astronomers to test our current models of stellar system formation and planetary formation.

The idea that planets beyond our solar system exist first appeared during the Copernican revolution in the 16<sup>th</sup> century. As astronomers were shifting from a geocentric to a heliocentric model, the Italian Giordano Bruno proposed that stars are just distant-suns that host systems similar to our solar system (Bruno 1584). The 16<sup>th</sup> century philosopher stated that "there may be an infinity of worlds similar to our own" and proposed the idea that life could exist elsewhere in the universe. Isaac Newton shared similar ideas while he was studying gravity. He also realized that stars were too far for the observation of alien worlds.

Detecting extrasolar planets was nevertheless greatly expected, especially after astronomers defined the mechanics behind the formation of our solar system. The most accepted model, known

as the solar nebular model, explains how the Sun formed from a giant and dense molecular cloud. As parts of the cloud fell together under gravitation, the densest region became a protostar. This protostar evolved into our Sun once fusion reactions began inside its core. The rotation of the young star flattened the cloud into a disk, allowing the formation of planets, asteroids and comets by accretion. This model successfully explains the formation of planets around our Sun and therefore also predicts the formation of planets around other stars.

With the progress of observing techniques and telescope design since the 19<sup>th</sup> century, many astronomers started to look for exoplanets but every single discovery claim was controversial until the 1990's. The first definitive detection of an extrasolar planet was in 1992, when radio astronomers Aleksander Wolszczan and Dale Frail announced the discovery of two planets orbiting the pulsar PSR 1257+12. A third planet around the pulsar was detected in 1994 but the origin of this system could not be fully determined. These planets could have formed from the remnant of the supernova who produced the pulsar, or it could be the remaining cores of planets orbiting the star before its supernova stage.

Finding a planet around a main-sequence star was the next step for astronomers. Main-sequence stars have not reached their catastrophic end-stages and are thus more likely to have planets orbiting them. In 1995, the astronomers Michel Mayor and Didier Queloz announced the first confirmed detection of an extrasolar planet around the star 51 Pegasi, a star similar to our Sun. The discovered planet, named 51 Pegasi b, is similar to Jupiter but orbits its star with a period of 4.23 days.

As more exoplanets were discovered in the early 2000's with extreme sizes and orbits, the International Astronomy Union (IAU) defined the criteria for extrasolar planets:

- objects with true masses below the limiting mass for thermonuclear fusion of deuterium (currently calculated to be 13 Jupiter masses for objects of solar metallicity) that orbit stars or stellar remnants are "planets" (no matter how they formed). The minimum mass/size required for an extrasolar object to be considered a planet should be the same as that used in the solar system.

- substellar objects with true masses above the limiting mass for thermonuclear fusion of deuterium are "brown dwarfs" , no matter how they formed or where they are located.
- free-floating objects in young star clusters with masses below the limiting mass for thermonuclear fusion of deuterium are not "planets", but are "sub-brown dwarfs" (or whatever name is most appropriate).

Later discoveries of exotic planetary bodies have challenged these definitions, making it hard to truly define the boundaries between planets, sub-brown dwarfs, brown dwarfs and stars. An alternate way to differentiate these objects is to look at the way they formed. Planets are formed by accretion in a stellar disk whereas stars, brown dwarfs and sub-brown dwarfs formed through the collapse of a gas cloud.

Since the first detection of an exoplanet 20 years ago, finding exoplanets has been one of the most dynamic fields of astronomy with 2038 discovered planets in 1291 different planetary systems, including 503 multiple planetary systems as of December 18<sup>th</sup>, 2015. Extrasolar planets greatly vary in size, mass and orbital period . They have challenged our understanding of planetary formation, migration and organization inside stellar systems, including our own solar system . The ultimate goal of exoplanet search is to find a planet similar to Earth in a planetary system similar to the solar system, where life is probable and potentially observable from Earth.

### 1.1.2 Detecting Methods

Exoplanets are extremely far and faint, making their detection very difficult, as written by a science journalist: "astronomers hoping to capture the light of an Earth-size planet around a star billions of times brighter compare the feat to picking a firefly from a searchlight's glare 3,000 miles (4,800 kilometers) away, on a foggy night" (Appenzeller 2004). Since a direct detection is nearly impossible, astronomers were forced to develop indirect detection methods by looking at the effect of the orbiting planet on its star's light. The first exoplanets were discovered using radial velocity ,

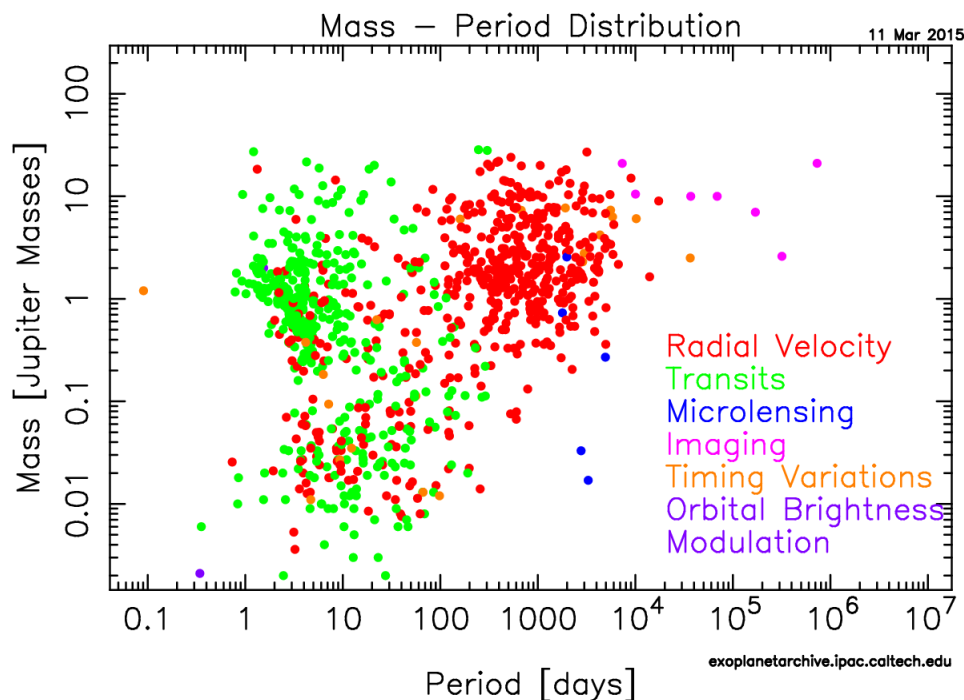


**Figure 1.1** The distribution of mass and period of all confirmed exoplanets

however, the transit method was used for most of the confirmed discoveries.

### Radial Velocity

A star and an orbiting planet will orbit their common center of mass. Since stars are much more massive than planets, the center of mass of a star-planet system is very close from the center of the star, however, we can still observe the star moving back and forth around this center of mass by measuring the radial velocity of the star. When the star is moving towards us, its spectra is blue-shifted under the Doppler effect. Similarly, when the star is moving away from us, its spectra is red-shifted. The color shift of a star gives us its radial velocity and a periodic variation of the radial velocity reveals the presence of an orbiting object. The period of the variation is simply the orbital period and the mass of the orbiting object is determined by the amplitude of the radial velocity variation.

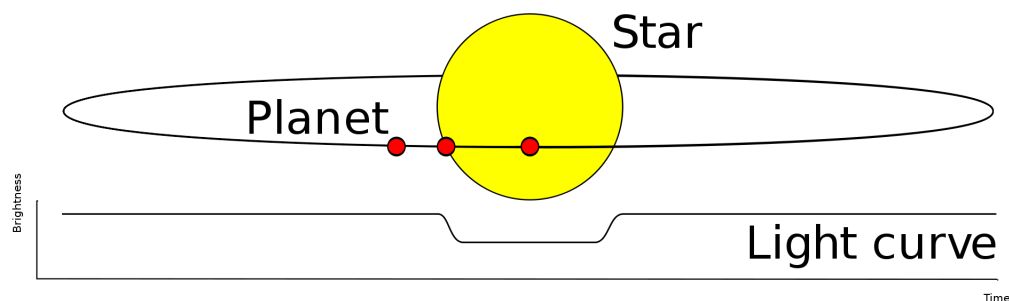


**Figure 1.2** A transiting planet will create a small dip in its parent stars light curve

Radial velocity was the first method used for planetary detection and one of the most successful. This technique is very efficient for detecting large planets orbiting low-mass stars, since they are more affected by their planet's gravity. Most planets found by radial velocity are gas giants with masses equal or greater than Jupiter's mass and with orbiting periods larger than 100 days (see Fig. 1.1).

### Transits

If a planet transits in front of its parent star, it will block a portion of the star's flux, creating a small periodic dip in the light curve (see Fig. 1.2). By measuring the depth and shape of the transit, the size and orbital period of the planet can be accurately estimated.

Despite being the most successful detection technique (see Fig. 1.3), the method only allows the detection of planets with an orbital plane aligned with our line of sight. If the inclination angle between the planet's orbit and our line of sight is too big, the planet will never be seen transiting from Earth. It also only allows the detection of planets close to their stars, as planets far from their stars transit less frequently and have a lesser probability to pass in front of their star. Therefore, most of the observed transiting planets are large gas giants with extremely short orbital periods (see Fig. 1.1). These planets are typically referred to as "hot Jupiters"

There are many more methods used for planetary detection, but none of them has been as

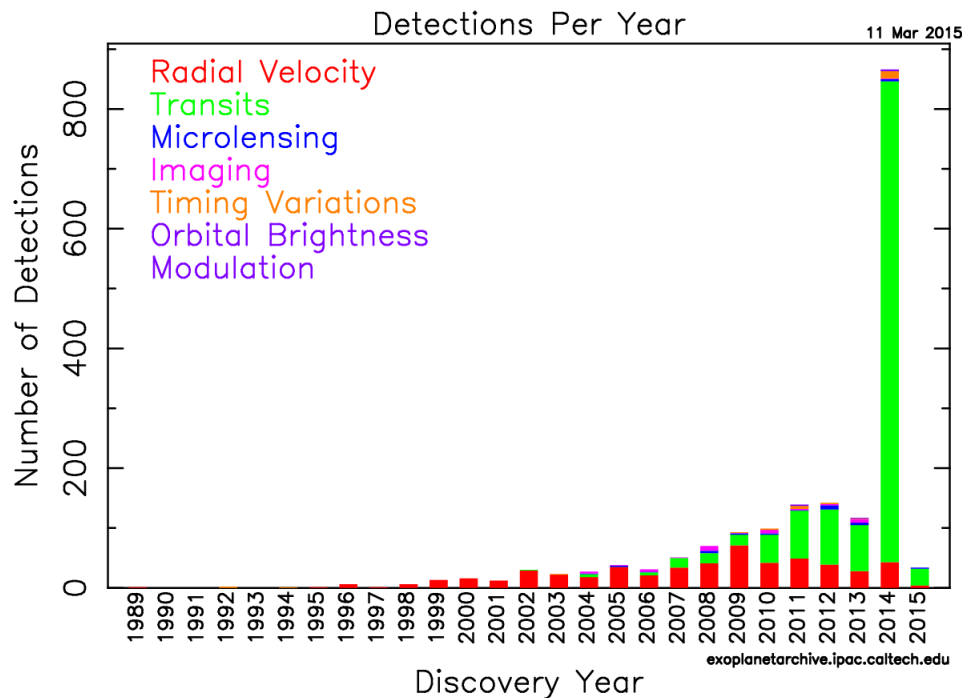


**Figure 1.3** The yearly distribution of discovered exoplanets by detecting method

fruitful as the radial velocity and transit methods.

## 1.2 M-dwarfs Systems

### 1.2.1 Physical Properties of M-dwarfs

M-dwarfs are main sequence stars that are cooler, smaller and less massive than our Sun. Main sequence stars are characterized by the thermonuclear fusion of hydrogen into helium in the stellar core. M-dwarfs have just about enough mass to create the necessary pressure and temperature that triggers fusion at the center of stars. Because of their low mass, thermonuclear fusion occurs at a slow rate. Meanwhile, the energy released by fusion is almost entirely transported to the stellar surface through convective cycles. This process carries helium, the product of fusion, away from the core and creates a steady flow of hydrogen into the core. With a constant and slow fusion rate,

M-dwarfs have a long lifespan but low luminosity .

The luminosity of stars is defined by:

$$L = 4\pi R^2 \sigma T^4$$

where R represents the radius of the star, T its surface temperature and  $\sigma$  is the Stefan-Boltzmann constant. Luminosity greatly depends on the temperature of the star. Consequently, no M-dwarf can be observed with the naked eye on Earth and their detection is challenging. The brightest M-dwarfs only have about 10% of our Sun's luminosity while the faintest emit as little as 0.00001% of the Sun's luminosity.

Luminosity is also be affected by starspots and stellar flares . Starspots are cooler regions on the surface of a star, where a concentration of magnetic field lines locally reduces the surface temperature. They frequently appear on the surface of M-dwarfs and can cover a significant portion of the surface. The light output of the star is then reduced for a period that can lasts a few weeks. Stellar flares are, in the opposite, sudden flash of brightness on the stellar surface. They are produced by the release of energy stored in the magnetic field. Some M-dwarfs are able to double their luminosity in a few minutes with giant flares.

### **1.2.2 M-dwarfs Habitable Zone**

The habitable zone is the region around a star within which planetary-mass objects with sufficient atmospheric pressure and temperature can support liquid water at their surfaces. The bounds of the habitable zone depends largely on the radiant energy received from the star. Since M-dwarfs are a lot less luminous than our Sun, the habitable zone around an M-dwarf is very close from the star. Then planets in the habitable zone have close orbits, so they are more likely to transit their star and if they do, their period will be short.

### 1.2.3 Abundance of M-dwarfs

Modern observations tools have allowed an increase of M-dwarfs observations in the recent decades, especially near our Solar System. In order to characterize the star population near our solar system, the Research Consortium on Nearby Stars (RECONS) has conducted multiple sky surveys. RECONS uses astrometric, photometric and spectroscopic techniques for detecting nearby stellar objects. The surveys have revealed that more than 75% of stars in the solar neighborhood (10 parsecs) are M-dwarfs (Henry 2006). The nearest star to our Solar system, Proxima Centauri, is an M-dwarf just 4.2 light-years away. Since the distribution of stars in our galaxy is mostly uniform, M-dwarfs are by far the most common stars in the Milky Way.

### 1.2.4 Abundance of Planets around M-dwarfs

The transiting method is by far the most successful at detecting Earth-like planets around M-dwarfs. However, since Earth's point of view of our galaxy does not change, only planets orbiting their star edge-on can be observed from Earth. Using the assumption that the angle distribution between our line of view and the orbit plane of a planet around its star is uniform, statistical analysis of the fraction of transiting planets detected around M-dwarfs show that the occurrence rate for Earth-size planets ( $0.5-4 R_{Earth}$ ) with orbital periods shorter than 50 days is  $0.90^{+0.04}_{-0.03}$ . Considering only the planets in the habitable zone, the occurrence rate drops to  $0.61^{+0.07}_{-0.15}$  (Kopparapu 2013). This occurrence rate results in an estimate 40 billions potential habitable Earth-like planets in our galaxy. It also makes M-dwarfs the most likely stellar type to have orbiting planets and Earth-like planets in the habitable zone.

## 1.3 Kepler Space Telescope

### 1.3.1 Mission and Purpose

Launch in 2009, NASA's Kepler space telescope was designed to detect and observe transiting planets. Its general objective is to explore the structure and diversity of planetary systems as defined by its given missions:

- Determine the abundance of terrestrial and larger planets in or near the habitable zone of a wide variety of stars
- Determine the distribution of sizes and shapes of the orbits of these planets
- Estimate how many planets there are in multiple-star systems
- Determine the variety of orbit sizes and planet reflectivities, sizes, masses and densities of short-period giant planets
- Determine the properties of those stars that harbor planetary systems

Kepler was successfully fulfilling its mission until two of its four reaction wheels broke in 2013. These reaction wheels were used to point the telescope during observations. The Kepler missions were nevertheless extended in 2014.

### 1.3.2 Observation Parameters

The Kepler space telescope is on an Earth-trailing heliocentric orbit. It is comprised of a 0.95 m aperture modified Schmidt telescope and a mosaic of 42 CCDs, each 2048 x 1024 pixels, covering a wide field (115 square degree). Observations are made in the wavelength range 430-890 nm. Kepler constantly monitored 150 000 main sequence stars between 8 and 15 mag in the Cygnus constellations, a region as far from the galactic center as the Sun (see Fig. 1.4). Measurements were made every 30 min for four years.

Kepler's data is publicly available after being processed by the official pipeline. The scientific

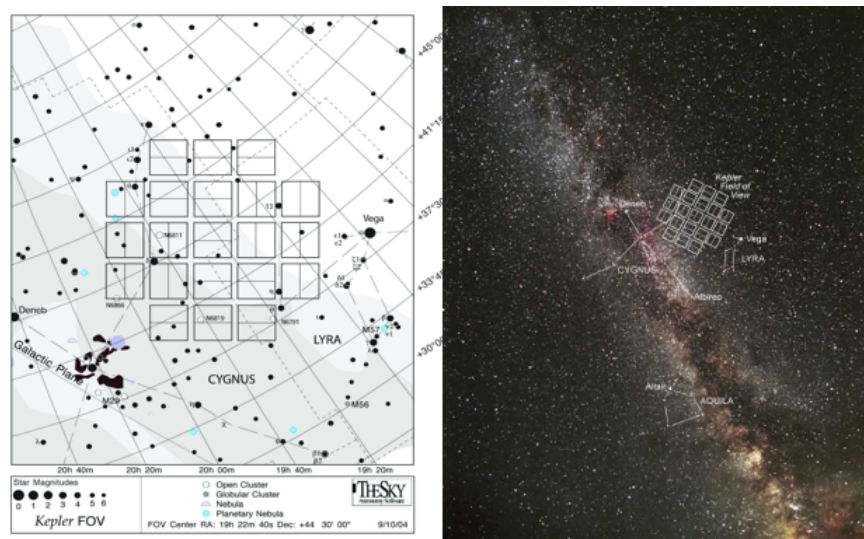


**Figure 1.4** Left panel: detailed map of Kepler’s field of view. Right panel: position of the field of view relative to the disk of the Milky Way.

community is invited to make follow-up observations in order to confirm or change the status of planetary candidate.

## 1.4 Observational Challenges to Transit Detection

### 1.4.1 Signal-to-noise Issues

The photometric objective for Kepler was a combined differential precision of 20 parts per million for a 12 mag star with an integration time of 6.5 hrs. This estimate was developed allowing 10 ppm for stellar variability, which corresponds to the variability of the Sun. The obtained accuracy for this observation has a wide range, depending on the star and position on the focal plane, with a median of 29 ppm. However preliminary results showed noise greater than expected (19.5 ppm) in the variability of the stars.

A greater noise level decreases the probability to detect small transiting planets as their transit signal is very close to the noise level. Instead of a predicted  $4\sigma$  value, an Earth-size transiting

planets has a  $2.7\sigma$  value, making it a harder detection.

### 1.4.2 Under-sampling

The Kepler space telescope is only measuring stars' brightness every 30 min. This cadence is considerably long for transiting events. For example, a two-hours transit would only consist of 4 low points, which does not give enough information about the transit length and depth. Under-sampling often reveals periodic signals that are less frequent because of the lack of low data points.

### 1.4.3 Transit Depth Limit

In order to detect a transit, the depth of the signal must be greater than the uncertainty brought by noise sources. Low-mass stars have a fainter signal and amplified natural noise levels. Detecting a transit is therefore harder for smaller stars. It requires a greater transit depth. The detection of Earth-size planets is then less likely for low-mass stars.

### 1.4.4 Light Pollution

The Kepler defined aperture consists of the pixels containing most of the target star's flux. The aperture may also contain light from neighboring stars. The additional flux from a star reduces the relative size of the transit depth of the original signal, making the resulting transiting planet smaller in size or undetectable.

## 1.5 Proposed Solution and Summary

In order to detect a planet transiting a M-dwarf, we must first clean its measured signal. We will first reduce external noise by modeling the star's light profile on Kepler's imaging instrument. We will then remove any trend created by the star's variability. Finally, a frequency analysis will reveal

the eventual presence of a transit. In Chapter 2 we will describe the method that we developed to increase the probability of a transit detection. Chapter 3 will discuss of the results we obtained with one Kepler target.

# Chapter 2

## Detection Method

Our detection method consists of three steps:

- reducing background noise with PyKE
- detrending the light curve from stellar variations with KepCurve
- detecting a transit signal by frequency analysis with Peranso

### 2.1 PSF Fitting with PyKE

#### 2.1.1 PyKE Introduction

Data gathered by the Kepler detectors is regularly downloaded and reduced into time-series by the Kepler pipeline. The Kepler data is automatically calibrated to remove trends brought by the spacecraft and its detectors. This systematic reduction was optimized to yield the highest number of potentially-detectable exoplanet transits from a sample of 200 000 stars of magnitude 14 or less. The resulting time-series are published in the Kepler Archive for further study. Since the Kepler pipeline focuses on sun-like stars, a lot of potential targets are automatically rejected.

Study of the rejected targets is nevertheless possible for the astronomy community as these

targets can potentially still show transiting events. The Kepler team has made available the time-series and individual pixel files of all targets, along with the specifically developed tool PyKE . This Python package is a group of tasks developed for the reduction and analysis of Kepler pixel-level data (Still 2012). PyKE was also developed to provide an alternative data reduction process, following the user's methods in order to fit specific target characteristics. The main purposes of these tasks are to re-extract light curves from manually-chosen pixel apertures and cotrend or detrend the data in order to reduce or remove systematic noise structure. Tasks to perform time-series analysis are also included. This open source software project is developed and distributed by the NASA Kepler Guest Observer Office. PyKE works as a PyRAF package and was first released in June 2010. It receives regular updates as the Kepler mission advances.

Our method focuses on three PyKE tasks: *kepfield*, *kepprf* and *kepprphot*.

### 2.1.2 Field Analysis with *kepfield*

The *kepfield* task plots the measured flux of each pixel within a target mask, provides positions of known stellar sources within and close to the mask, and defines the photometric aperture chosen by the Kepler pipeline. This plot provides the necessary information for understanding the fraction of target flux that falls within the pipeline photometric aperture and potential sources of contaminating flux from nearby sources falling within the aperture. The resulting plot can be used to choose whether a new light curve is worth constructing from a point spread function (PSF) fitting.

The *kepfield* task also produces a table associated to the target's field. For each star in the field, the table contains the CCD position of the star's center, its coordinates, and its magnitude. The table lists the identification number of each star in the Kepler and 2MASS catalog. Since these two catalogs were independently created, most of the Kepler stars are also identified in the 2MASS catalog. The same stars can therefore appear twice in the *kepfield* output. With the use of an astronomy catalog database such as the Set of Identifications, Measurements, and Bibliography

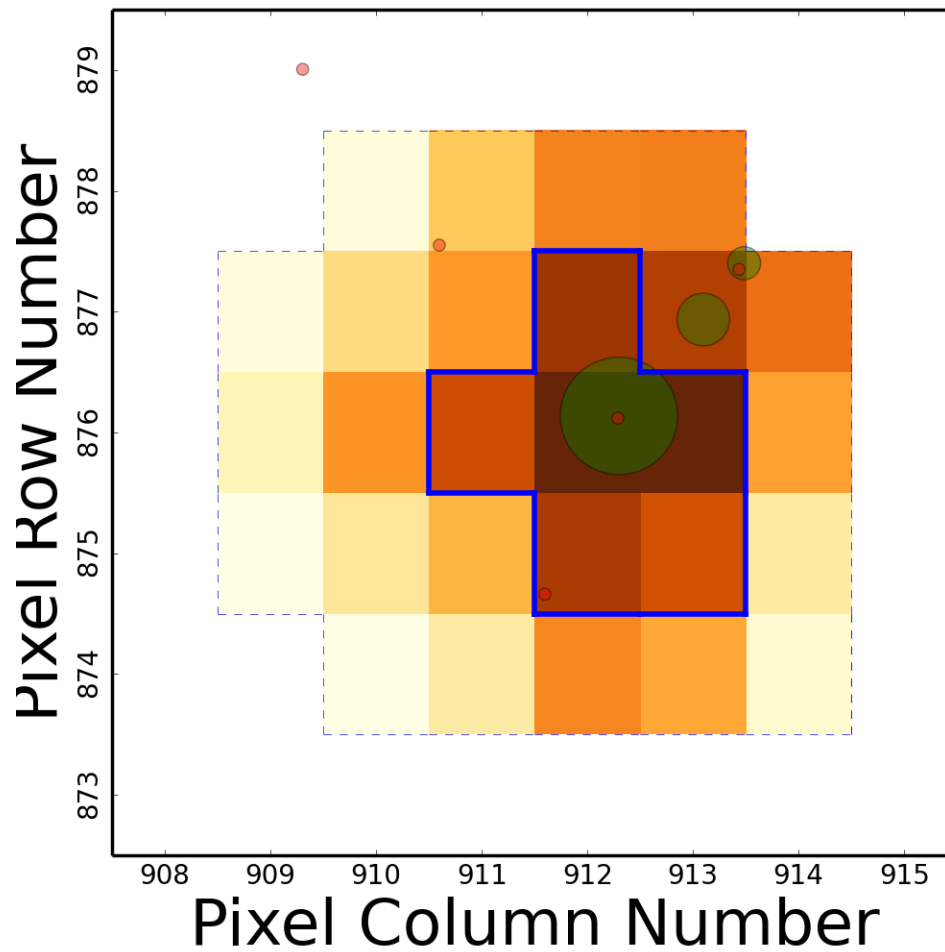


**Figure 2.1** The field of a star around a Kepler target is shown with the Kepler photometric aperture. The green disks represent Kepler targets, the red dots are known stars from the 2MASS catalog and the blue line represents the aperture used by the Kepler pipeline, revealing the potential for light pollution

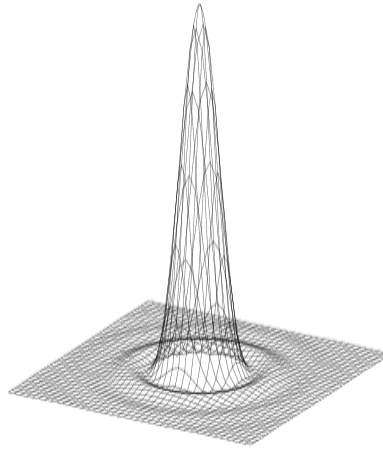


**Figure 2.2** PSF model of a typical star as recorded by a traditional CCD

for Astronomical Data (SIMBAD) found at <http://simbad.u-strasbg.fr/simbad/>, repeated stars in the output can be ignored and be differentiated from stars with fluxes falling within the aperture.

Fig. 2.1 is a graphical representation of the table output. Each square represents a pixel on the Kepler CCD array with color corresponding to the relative intensity of the flux measured. Green disks represents stars from the Kepler catalog while red disks represent stars from the 2MASS catalog. In this example, two of the Kepler stars are also known in the 2MASS catalog. The size of the green disks is proportional to the measured magnitude of the star. The blue line defines the border of the photometric aperture chosen by the Kepler pipeline.

In this example one can see that the aperture might not contain all of the flux from the target star (large green disk situated inside the aperture). The aperture might also contain parts of another star's flux (situated in column 913, row 877). Both stars affect the target's measured flux.

### 2.1.3 Modeling the Field with *kepprf*

The *kepprf* task fits a PSF model (see Fig. 2.2), combined with spacecraft jitter, pixel scale drift and pixel response function (PRF) models to a single frame of a Kepler target pixels.

The PRF depends on the optical design, focus setting, CCD detector mechanical and electronic

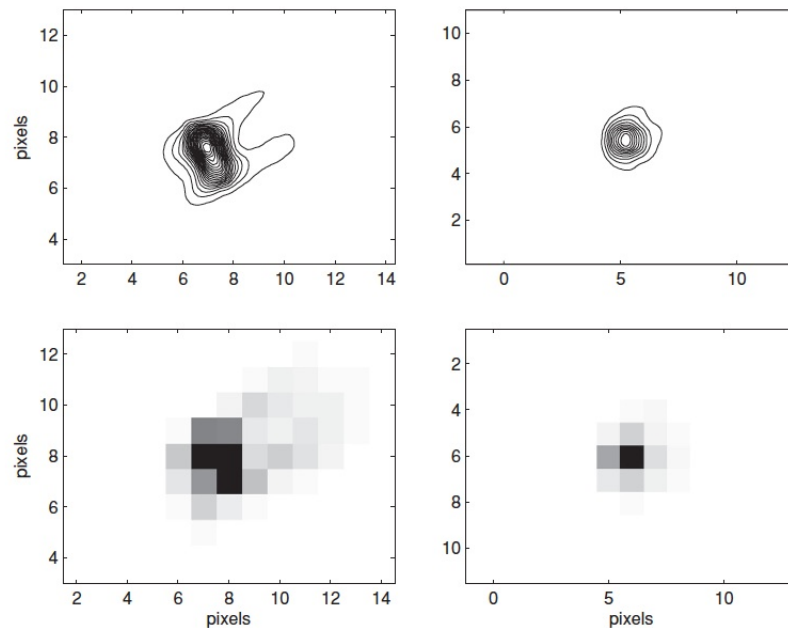


**Figure 2.3** Representation of the PRF at two locations in the focal plane. On the left: a PRF from near the edge; on the right: a PRF near the center. The pixelated image is shown below and a contoured version above.

properties, and the temporal sequence of spacecraft pointing stability during an observation. The PRF quantifies the total response of the instrument to incident light from a point source in terms of its individual pixel reaction. The Kepler PRF varies for each individual pixel and depends on the location of the peak of the light source (see Fig. 2.3). PRF models for Kepler were obtained from calibration frames taken before Kepler’s first observations. The resulting PRF models are then used to build a PSF representing how light from a star spreads on the CCD pixels.

*kepprf* asks for pixel coordinates of each star to consider for a fit. It finds the exact center of the stars’ PSF and estimates their relative flux. The task finds the best PRF model and creates a PSF for each star. The output of *kepprf* consists of 4 different pixel images of the targeted field (see Fig. 2.4). The first image (top left) shows the actual flux measured by the detectors. The second image (top right) is the combined PSF models that yield the best fit to the selected stars found with *kepprf*. The third image (bottom left) is a pixelated representation of the best-fit model,

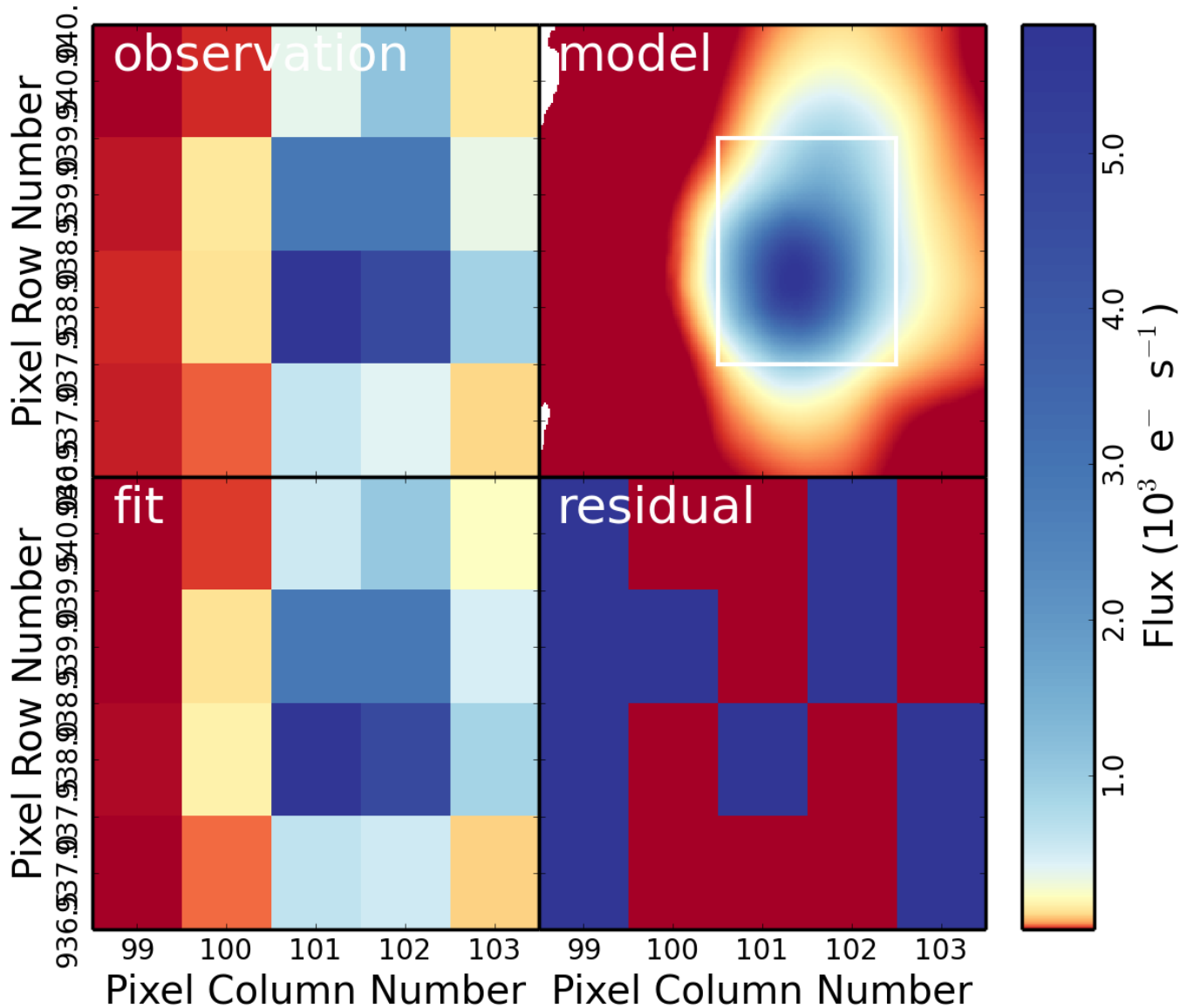


**Figure 2.4** *kepprf* finds the best PSF fit to selected stars in the target field. Top left: actual flux measured by the CCD. Top right: combined PSF models that yield the best fit. Bottom left: pixelated representation of the best-fit model. Bottom right: residual after subtracting the best fit from the real data.

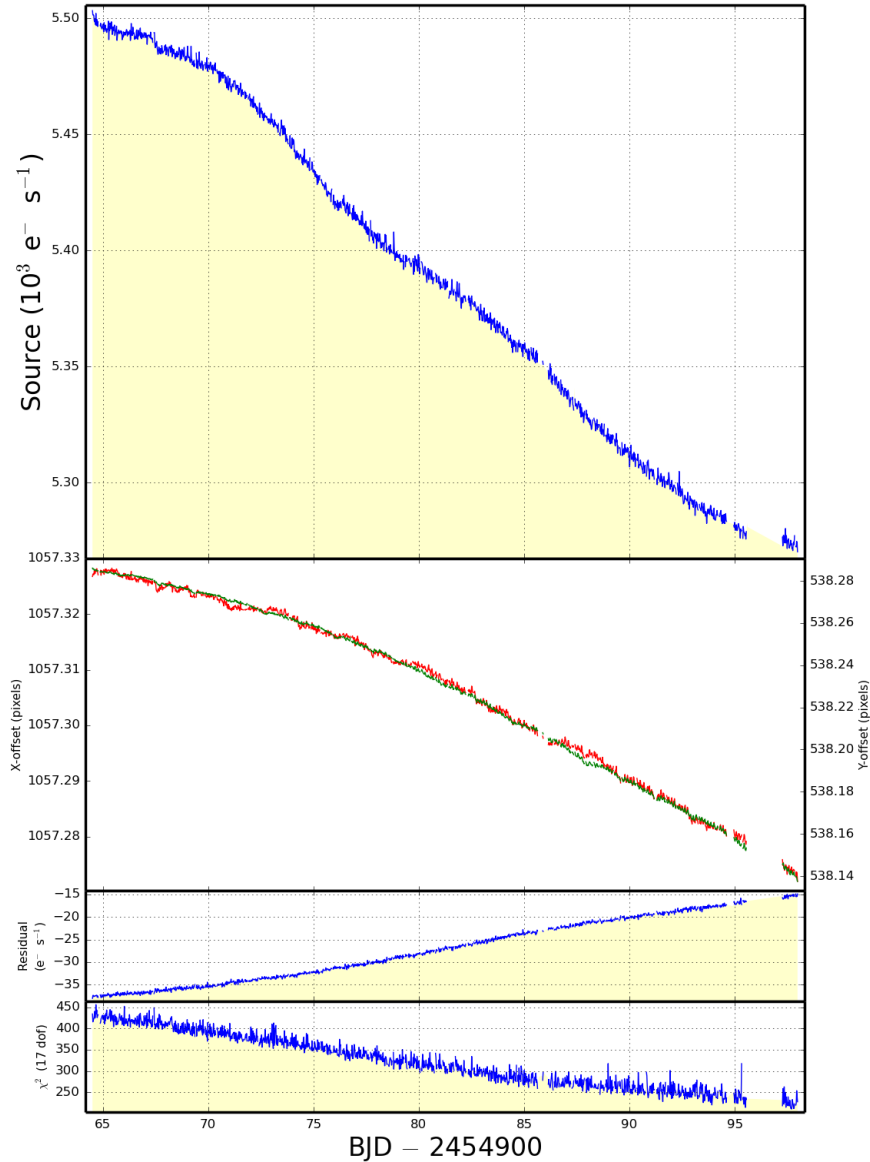


**Figure 2.5** *kepprfphot* extends the best PSF fit to a full time series. First panel: new photometric curve obtained from the best PSF fit. Second panel: drift in the  $x$  and  $y$  directions of the center of the star's PSF as a function of time. Third panel: residual flux left by the model. Fourth panel: measure of the goodness of the fit ( $\chi^2$ ). Note: the Barycentric Julian Date (BJD) is the Julian Date (JD) corrected for differences in the Earth's position with respect to the barycentre of the Solar System.

interpolated from the PSF. The fourth image (bottom right) is the residual after subtracting the best fit from the real data. Finding the best fit depends on the star selection and the initial guess for the relative flux between the stars. Once a satisfying fit is found (low residual), the model can be applied to the rest of the time-series.

#### 2.1.4 Obtaining a New Time Series with *keprfphot*

The *keprfphot* task repeats the *keprf* task on every frame in the time-series. It then derives a new photometric light curve from the best-fit model found with *keprf*. This light curve presents reduced noise from background stars and spacecraft jitter.

The output from *keprfphot* consists of 4 distinct plots (see Fig. 2.5). The top plot is the new photometric curve obtained from the best PSF fit. It shows flux measured against time. The second plot shows the drift in the  $x$  and  $y$  directions of the center of the star's PSF as a function of time. The last two plots are a measure of the residual and fit quality. Fig. 2.5 shows the light curve of a Kepler target over a full quarter (3 months). The star's flux seems to decrease over the quarter, but it is only a trend brought by the drift of the star on the CCD.

## 2.2 Detrending the Time Series with KepCurve

Photometry of the best-fit model can only reduce background noise. M-dwarfs have large brightness variations, making it difficult to extract a transiting signal. Detrending is needed to process the time series by detecting and suppressing trends. The software KepCurve was specifically developed for detrending Kepler light curves. It models trends in the time series and creates a residual time-series for study (see Fig. 2.4).

Detrending detects the slow and gradual changes over the entire series. Piece-wise functions are used to fit the curve as it slowly varies. Since detrending only focuses on low frequency variations,

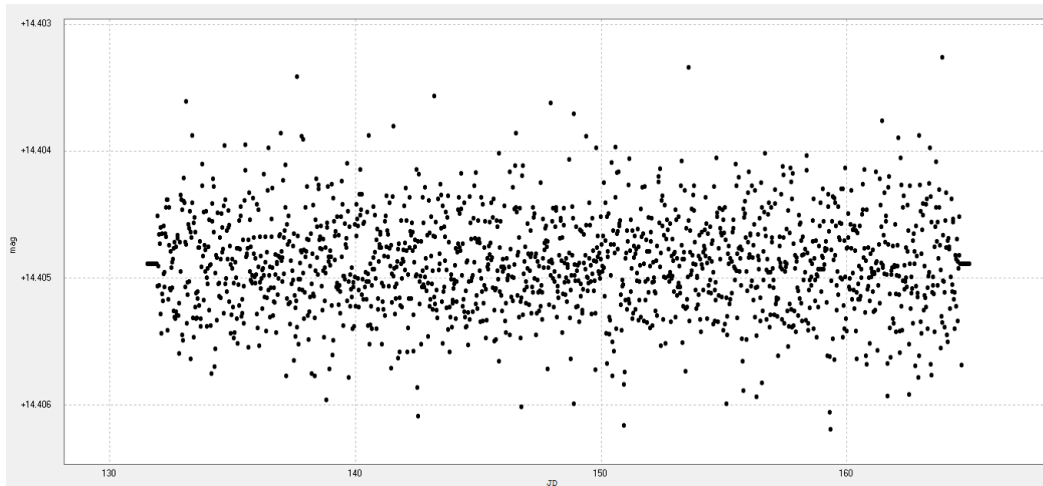


**Figure 2.6** A detrended time-series does not show any long-period variations.

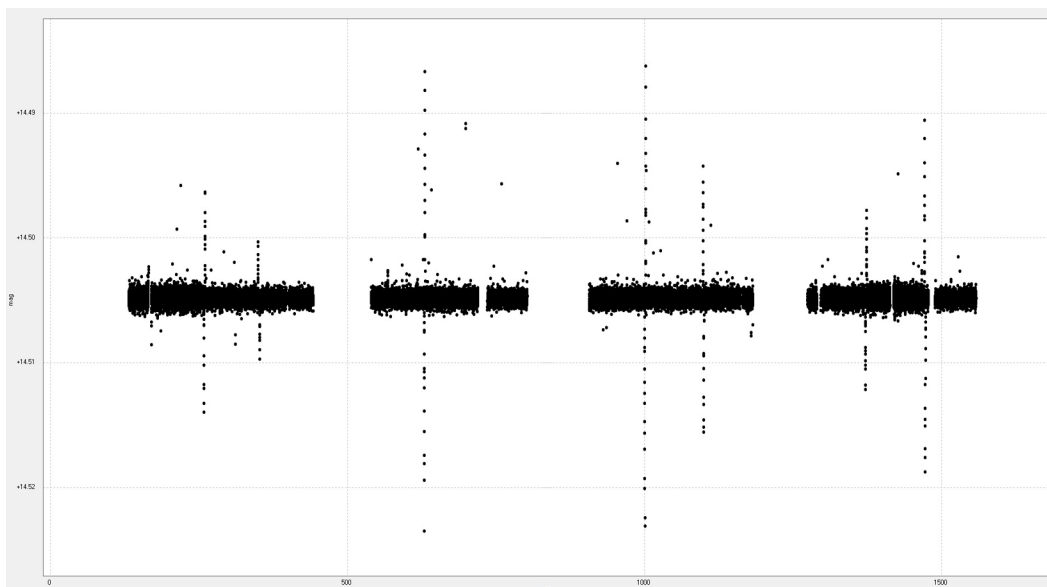


**Figure 2.7** Merged data from 14 quarters. Non-transiting single events were not removed.

a relative short dip in the light curve is ignored by the fitting process. Trends are removed by taking the ratio of the time series to the trend line at every point in time. The ratio will exceed one when the series is above the trend line and will be below one when the series is below the trend line.

Detrending also fixes discontinuity in the time series due to quarter change or telescope rotation. Multiple quarters are usually available for most Kepler targets. After obtaining and detrending new time series for each quarter, KepCurve will merge the time series and level them for period analysis (see Fig. 2.7).

Finally, the last type of non-transit variations to remove from the data before period analysis are short, single events such as star flare or star spots . These data points are relatively far from the final trend line and are easily cut from the data by removing all data points above or below a certain level.

## **2.3 Detecting Transits with Peranso**

Peranso is a software developed by the CBS Belgium Observatory (Kovacs 2002). It offers a complete set of light curve and period analysis functions to work with large sets of observations like Kepler data.

### **2.3.1 Period Analysis**

Peranso uses the Edge Enhanced Box-fitting Least Squares (EEBLS) period analysis method for detecting transiting events. Box-fitting Least Squares (BLS) algorithms are particularly effective to analyze stellar photometric time series in search for periodic transits by exoplanets. It searches for signals characterized by a periodic alternation between two discrete levels, with much less time spent at the lower level. EEBLS is an extension to BLS that takes into account edge effects at the start and end of the ingress and egress portion of a planetary transit.

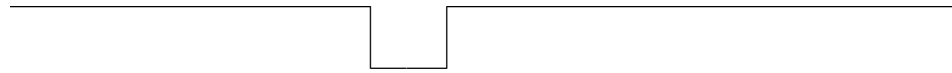


**Figure 2.8** A targeted signal in an EEBS period analysis

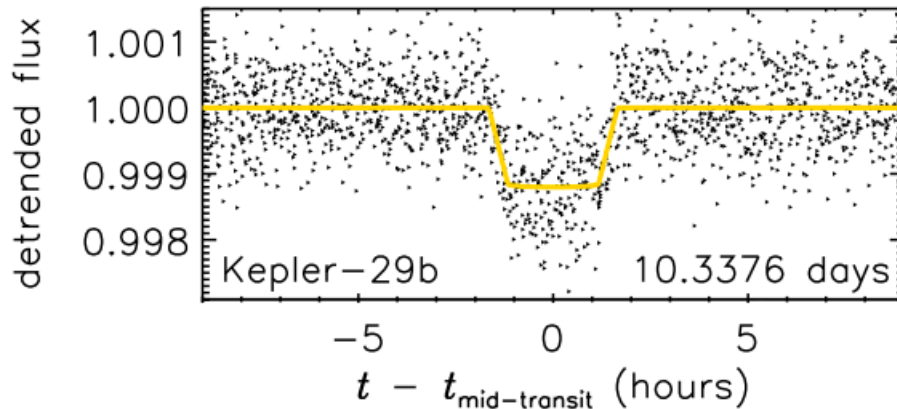


**Figure 2.9** Example of a phase plot for a planet found by Kepler.

Peranso runs an EEBS analysis over a selected window of period or frequency. The resulting frequency spectrum shows the most dominant EEBS periods.

### 2.3.2 Phasing

Peranso calculates the reference time (epoch) of mid-transit events and phase the entire data set for the dominating period. Phasing cuts the time-series according to the dominating period and folds every pieces together, creating a superposition of all data points over one period. If there is a transit, the superposition of data points reveals a short dip in the flux (see Fig. 2.9). If no transit is apparent, the inconclusive frequency can be ignored and the analysis is repeated until a periodic transit is found or no dominant periods yield to a transit event.

If a transit is observed, Peranso displays the depth and length of the transit, which are used to calculate the size and orbit distance of the exoplanet.

# Chapter 3

## Results

### 3.1 Target Parameters

#### 3.1.1 Parameters

There are thousands of stars in the Kepler stellar catalog. In order to identify the M-dwarfs, we used general values of the surface temperature, radius and mass of M-dwarfs (see Table 3.1). To select our targets, the lower bound of our magnitude range was chosen where the Kepler pipeline starts to be less efficient at detecting planets while the upper bound was chosen to guarantee a short list of relatively bright stars

Magnitude	14-14.5
Temperature	<3800 K
Radius (Sun)	<0.60
Mass (Sun)	<0.62
Confirmed Planets	0

**Table 3.1** Kepler Stellar Table Parameters

With these parameters, 113 target stars were selected for our analysis.

### 3.1.2 Kepler’s Pipeline Results

Among the 113 target stars, 12 of them had one or more transit-like events (TCE) detected by the automated Kepler pipeline and 6 had a Kepler Object of Interest (KOI) . The Kepler team requires the detection of multiple transit-like events before giving a star a KOI. We decided to test our method with stars showing potential transit. We eliminated targets that did not have any close neighbors in their photometric aperture or produced discontinuous time-series. One target, KepID 5080636, produced continuous, low-noise time-series. We chose to focus on this star.

## 3.2 Results for KepID 5080636

### 3.2.1 Stellar Properties

This M-dwarf is a 14.4 mag star and is a little less than half the size and mass of the Sun (see Table 3.2). Stellar properties were derived from temperature analysis of a combined Kepler and 2MASS catalog (Pinsonneault 2012).

<i>Magnitude</i>	14.404
<i>Temperature(K)</i>	$3584^{+69}_{-54}$
<i>Radius<sub>Sun</sub></i>	$0.45^{+0.08}_{-0.05}$
<i>Mass<sub>Sun</sub></i>	$0.464^{+0.08}_{-0.05}$

**Table 3.2** KepID 5080636 Properties

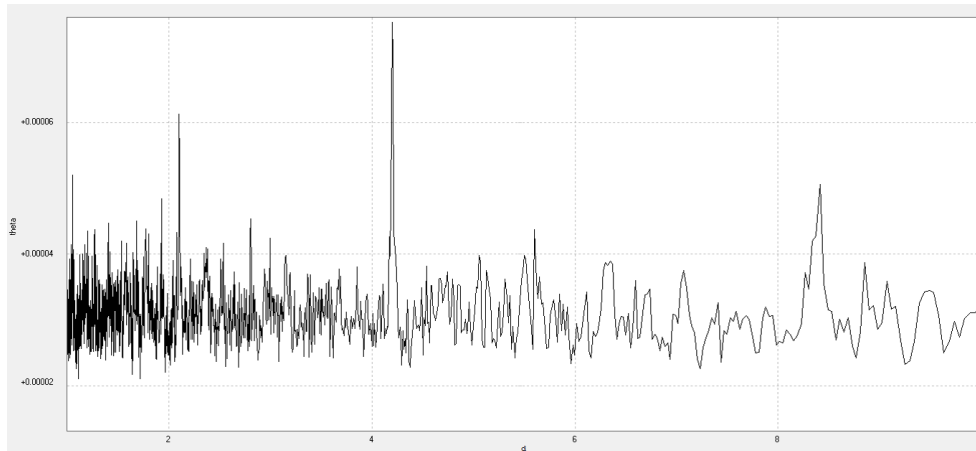


**Figure 3.1** This Fast Fourier Transform (FFT) shows prominent periods from the time-series. Period length is found on the x-axis while the transform power is on the y-axis. The two prominent periods found are 4.19 days and 2.10 days. No noticeable periods were found around 6.3 days.

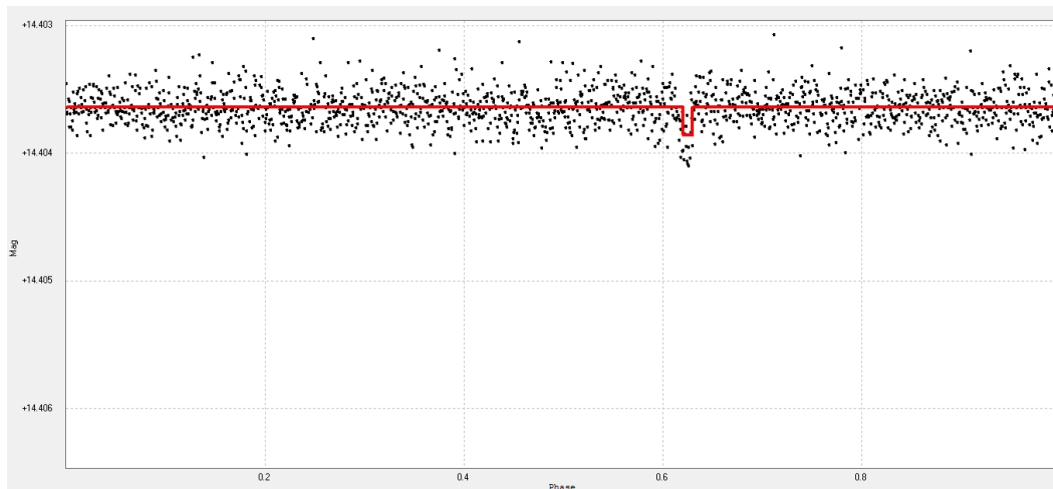


**Figure 3.2 ]**

Phased light curve from an individual quarter. The phased data shows an apparent transit at a 4.19 days period. The red line is the EEBS fit.

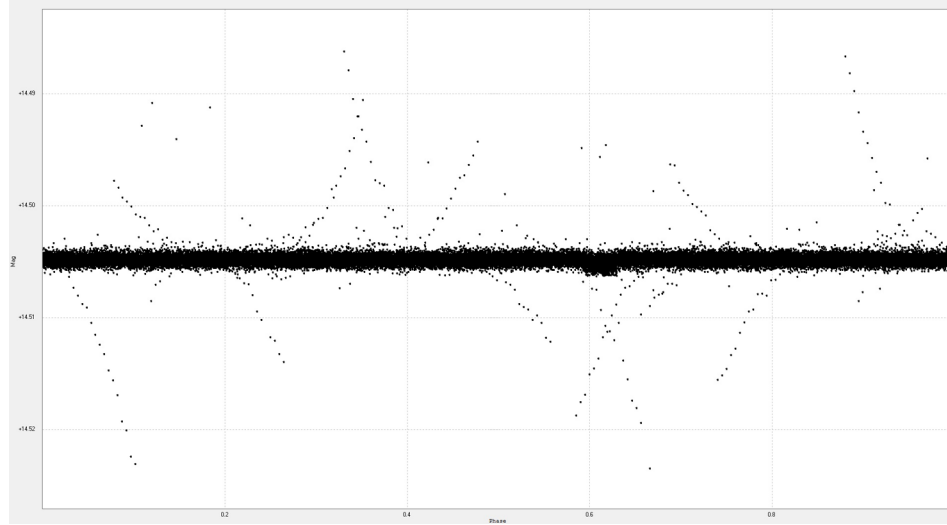


**Figure 3.3** Phased light curve from all available quarters. The combination of all quarters allows for a better estimation of the transit length: 2.4 hours.

### 3.2.2 Transit Detection

A transit was detected at a period of 4.19 days (see Fig. 3.1) and transit length 2.4 hours over the entire set of quarters available (see Fig. 3.2 & Fig. 3.3). The transit depth is 730 ppm or 0.086%.

Using the following equations, we were able to calculate the orbital radius of the planet and its approximate size:

- Orbit distance from Kepler's Third Law:  $a \approx \left( GM_* \left( \frac{P}{2\pi} \right)^2 \right)^{\frac{1}{3}}$  where  $G$  is the gravitational constant,  $M_*$  is the mass of the star and  $P$  is the orbiting period .

- Radius of the planet from transit depth  $\Delta F$ :  $\frac{\Delta F}{F} = \frac{R_p^2}{R_*^2}$  where  $F$  is the flux.

The candidate planet has a radius between  $1.28 R_{Earth}$  and  $1.70 R_{Earth}$ . Its orbit is estimated between 0.0379 AU and 0.0415 AU

### 3.2.3 Planet Properties

The equilibrium surface temperature of the planet can be estimated from balancing the energy absorbed and emitted by the planet:  $T_p = \left( \frac{R_*}{a} \right)^{1/2} \left( \frac{1-A}{4} \right)^{1/4} T_*$  where  $A$  is the albedo of the planet.

For an Earth-like planet ( $A = 0.3$ ), the temperature is estimated between  $483K$  and  $602K$ . If the planet is more like Venus or a gas giant ( $A = 0.7$ ), the temperature is estimated between  $391K$  and  $487K$ . These equilibrium temperatures are too high for liquid water to flow on the surface of a planet with an Earth-like atmosphere, however, liquid water could exist under the right atmospheric conditions. In terms of the temperature range, this planet is just inside the habitable zone .

### 3.3 Comparison and Future Work

We found a potential planet with a 4.19 days period and a transit length of 2.4 hours. Recent work has confirmed our findings and our candidate has become KOI 1843.01 after it was detected by the Kepler pipeline with a similar period but shorter transit length (1.8 hours).

The Kepler pipeline has also detected one KOI with a 6.3 days period (KOI 1843.02). Our analysis shows that this potential planet is a false positive. The second most dominant period on the frequency spectrum is at 2.1 days period, exactly half the period of 1843.02. This frequency is an "echo" of the 4.2 period as it does present a real transit every other period. The 6.3 days period is also a build-up of the 2.1 and 4.2 periods. Our phase plot at 6.3 days does not show any transit-like events.

A survey for short-period planets in the Kepler data using an EEBS algorithm detected transiting events at the 6.3 days period (Jackson, 2013). Since the survey specifically looked for planets with periods less than 0.5 days, no further study was made for this potential planet. The existence of 1843.02 remains debatable.

Our method was successful at independently detecting a potential transiting planet. Some of our results agree with research done by other teams. Our analysis shows that one candidate is a false positive, but this result is not confirmed by other teams.

There are still 112 targets in our sample, including a dozen planetary candidates. Work can be

done on these objects in order to see if our method can consistently detect exoplanets , but also to find why some of our results do not agree with work done with methods similar to ours.

The study of Kepler stars can also be extended to flares and star spots. After reducing external noise, these events are prominent features in time-series. Understanding the surface activity of M-dwarfs helps the modeling of the stellar interior of these common stars. Furthermore, these events could influence the potential for life on planets orbiting M-dwarfs.

# Appendix A

## Kepler Stellar Table

Kepler ID	2MASS ID	Mag	T(K)	R(Sun)	M(Sun)	KOI	TCE
9004474	J18571765+4520464	14	3723	0.46	0.47	0	0
8414216	J18563791+4427327	14	3787	0.51	0.51	0	0
2577743	J19272630+3753469	14.01	3661	0.56	0.56	0	0
4904647	J18592787+4001300	14.02	3661	0.56	0.56	0	0
4173772	J19412016+3912129	14.03	2979	0.14	0.11	0	0
8218687	J19011420+4411288	14.03	3608	0.42	0.44	0	0
4581084	J19453730+3937422	14.03	3337	0.18	0.16	0	0
3438817	J19201826+3830254	14.03	3651	0.5	0.52	0	0
6019923	J18501669+4120486	14.04	3530	0.38	0.4	0	0
8381383	J19481506+4419545	14.04	3784	0.49	0.49	0	0
4655612	J19275318+3942375	14.04	3718	0.41	0.43	0	0
11669367	J19423067+4942340	14.04	3566	0.38	0.4	0	0
8168452	J19311383+4402268	14.04	3622	0.39	0.4	0	0
7871438	J18512731+4340282	14.05	3757	0.49	0.5	0	6

8111203	J19451519+4359191	14.06	3666	0.43	0.45	0	0
4731525	J19062452+3952577	14.06	3421	0.35	0.36	0	0
8297629	J19240460+4416563	14.06	3530	0.38	0.4	0	0
11612409	J19310135+4940442	14.06	3661	0.43	0.44	0	0
6345048	J18565215+4145431	14.06	3630	0.39	0.41	0	0
7219652	J19475137+4242353	14.06	3785	0.5	0.52	0	0
5791720	J19281782+4104122	14.07	3702	0.57	0.57	0	0
8463121	J20063664+4428286	14.07	3705	0.48	0.49	0	0
4036313	J18592677+3911371	14.08	3455	0.33	0.33	0	0
7878428	J19062555+4336239	14.09	3681	0.46	0.47	0	0
7955545	J19210643+4347472	14.1	2661	0.12	0.09	0	0
11389341	J18543941+4915349	14.12	3617	0.4	0.42	0	0
10615211	J19490461+4750273	14.12	3702	0.57	0.57	0	0
12505054	J19130891+5127421	14.13	3521	0.35	0.36	0	0
9077376	J19055875+4528444	14.14	3772	0.5	0.51	0	0
12314646	J19412234+5104273	14.14	3444	0.32	0.32	0	0
12004872	J19061507+5029221	14.15	3514	0.37	0.39	0	4
9991488	J18441633+4658288	14.15	3404	0.34	0.34	0	0
8888573	J19314700+4506148	14.18	3687	0.56	0.57	0	0
9753740	J18504901+4630190	14.18	3799	0.49	0.5	0	0
8112537	J19465045+4359264	14.2	3661	0.56	0.56	0	0
6921817	J18440947+4229110	14.2	3619	0.43	0.44	0	0
3116544	J19254918+3817461	14.21	3795	0.47	0.48	0	0
8607535	J18542935+4444008	14.21	3345	0.29	0.28	0	0

11852982	J18595966+5008484	14.22	3741	0.49	0.51	1	1
3748918	J19274797+3851538	14.22	3747	0.47	0.48	0	0
7105834	J19112094+4238474	14.22	3316	0.27	0.25	0	0
10597927	J19240635+4752353	14.23	2661	0.12	0.09	0	0
5858361	J19000393+4109460	14.23	3498	0.36	0.37	0	0
5268904	J19194614+4028248	14.24	3403	0.34	0.34	0	0
8564323	J19341023+4437212	14.24	3749	0.45	0.46	0	0
3940072	J19074772+3901525	14.24	3687	0.56	0.57	0	0
7939565	J18501597+4345164	14.25	3296	0.22	0.2	0	2
10454036	J18562773+4739444	14.25	3737	0.47	0.48	0	0
6185476	J18572448+4131091	14.27	3745	0.47	0.49	1	8
8408875	J18435706+4426241	14.27	2923	0.14	0.11	0	0
10990886	J19522536+4824041	14.27	3744	0.5	0.52	1	1
6921821	J18440986+4229062	14.28	3417	0.35	0.35	0	0
9579672	J19113804+4615586	14.28	3584	0.45	0.46	0	0
4735754	J19132759+3949455	14.28	3677	0.44	0.45	0	0
11124203	J18564713+4846047	14.29	3600	0.42	0.43	0	0
4946433	J19491908+4005589	14.29	3606	0.35	0.36	0	0
10850518	J19065103+4812132	14.3	3758	0.47	0.49	0	0
9201919	J18534156+4539507	14.31	3773	0.5	0.51	0	0
11446732	J19080323+4920154	14.33	3436	0.32	0.32	0	0
12203198	J19130649+5051031	14.34	3772	0.48	0.49	0	0
6928206	J18564210+4227408	14.35	3699	0.47	0.48	0	0
4770707	J19495824+3952116	14.35	3469	0.32	0.31	0	0

5951140	J19153323+4114482	14.35	3582	0.41	0.43	0	7
9093501	J19341192+4525420	14.36	3522	0.41	0.43	0	0
8233490	J19272420+4407393	14.37	3735	0.44	0.46	0	0
8393582	J20004129+4423388	14.38	3772	0.33	0.34	0	0
3946894	J19172180+3902017	14.38	3658	0.45	0.46	0	0
11802278	J18590831+5001443	14.39	3728	0.48	0.49	0	0
9833329	J19312019+4641429	14.39	3686	0.44	0.46	0	0
9651052	J19302427+4618233	14.4	2940	0.14	0.11	0	0
11862267	J19232301+5009570	14.4	3539	0.42	0.44	0	0
8052057	J19544554+4351064	14.4	2661	0.12	0.09	0	0
8008320	J18501190+4352076	14.4	3629	0.43	0.45	0	0
5080636	J19000314+4013147	14.4	3584	0.45	0.46	2	2
10224595	J19504135+4713126	14.41	3250	0.2	0.18	0	0
10525990	J19112446+4744309	14.41	3780	0.46	0.47	0	0
12689927	J19173884+5149426	14.41	3598	0.42	0.44	0	0
10328903	J19075115+4729474	14.41	3661	0.4	0.42	0	0
10938188	J19554490+4820034	14.42	3498	0.36	0.37	0	0
6125019	J19290855+4129489	14.42	3746	0.47	0.48	0	0
8217295	J18580896+4411371	14.42	3434	0.36	0.37	0	0
6047929	J19340162+4121013	14.42	3630	0.44	0.46	0	0
11086755	J19324456+4840332	14.42	3632	0.44	0.45	0	0
5252367	J18524653+4029442	14.43	3316	0.27	0.25	0	0
5895919	J19481619+4108147	14.44	3715	0.45	0.47	0	1
9691974	J18473898+4629083	14.44	3522	0.41	0.43	0	0

10779603	J18532042+4808487	14.44	3725	0.39	0.41	0	0
11521274	J19512666+4924527	14.45	3482	0.35	0.36	0	0
6224062	J19475480+4135302	14.45	3707	0.45	0.46	0	5
7800087	J18460555+4332131	14.45	3638	0.44	0.46	0	0
9713353	J19322874+4624456	14.46	3677	0.41	0.43	0	0
7802933	J18525882+4335391	14.46	3699	0.47	0.48	0	0
12122143	J19482010+5038442	14.46	3682	0.46	0.47	0	0
7871442	J18512815+4340142	14.46	3780	0.46	0.47	0	0
6497146	J18463499+4157039	14.47	3688	0.46	0.48	1	1
8487692	J19153071+4432248	14.47	3546	0.39	0.41	0	0
9020510	J19251501+4518091	14.47	3767	0.48	0.49	0	0
11308755	J19474843+4900324	14.47	3497	0.26	0.26	0	0
9580721	J19135773+4615535	14.47	3710	0.43	0.45	0	0
12060710	J19233077+5035350	14.47	3598	0.42	0.44	0	0
11925804	J19485718+5015245	14.48	3715	0.44	0.45	0	0
4909186	J19075388+4001230	14.48	3304	0.26	0.24	0	0
8082910	J19015426+4356256	14.48	3699	0.47	0.48	0	0
11297141	J19274991+4900423	14.48	3482	0.35	0.36	0	0
5201711	J19424627+4023576	14.48	3749	0.43	0.44	0	0
9992083	J18460421+4658428	14.48	3761	0.53	0.54	0	0
9390653	J18594123+4558206	14.49	3514	0.37	0.39	1	1
3426367	J19034293+3831155	14.49	3410	0.35	0.35	1	1
4355120	J19150031+3929464	14.49	3552	0.39	0.41	0	0
5340107	J18530126+4032134	14.49	3713	0.43	0.45	0	0

---

5855851	J18545905+4109211	14.5	3279	0.24	0.22	0	0
5304146	J19544387+4025193	14.5	3279	0.24	0.22	0	0
7830341	J19375087+4331282	14.5	3799	0.49	0.5	0	0

---

**Table A.1** Kepler Stellar Table

The list of 113 targets (see Table A.1) was obtained with values for M-dwarfs (see Table A.2) from the Kepler Stellar Table found at <http://exoplanetarchive.ipac.caltech.edu/index.html>

Magnitude	14-14.5
Temperature	<3800 K
Radius (Sun)	<0.60
Mass (Sun)	<0.62
Confirmed Planets	0

**Table A.2** Kepler Stellar Table Parameters

# Bibliography

Bruno G., *"On the Infinite Universe and Worlds"*, 1584

Appenzeller T., *"Search For Other Earths"*, National Geographic, December 2004

Henry T., Jao W., Subasavage J. et al., *"The Solar Neighborhood. XVII. Parallax Results from the CTIOPI 0.9 m program"*, ApJ, 132:2360, December 2006

Kopparapu R., *"Habitable Zones Around Main-Sequence Stars: New Estimates "*, ApJ, Mars 2013

Still M., Barclay T., *"PyKE: Reduction and analysis of Kepler Simple Aperture Photometry data"*, ASCL, 2012

Kovacs G., *"A box-fitting algorithm in the search for periodic transits"*, A&A 391, 2002

Pinsonneault M., An D., Molenda-Zakowicz J., *"A Revised Effective Temperature Scale for the Kepler Input Catalog"*, ApJ Suppl., 199:30, 2012

# Index

*kepfield*, 14  
*kepprfphot*, 20  
*kepprf*, 16

brown dwarf, 3

detrend, 20  
Doppler effect, 4

EEBLs, 22  
epoch, 23  
exoplanet, 1, 3, 9, 29

flare, 7, 22  
Fourier transform, 26

habitable zone, 7, 28

KepCurve, 20  
Kepler, 9, 13  
Kepler object of interest, 25

luminosity, 7

M-dwarfs, 6, 8, 24  
main sequence, 2

Peranso, 22  
period, 2, 3, 5, 23, 26, 27  
phase plot, 23, 26  
pixel response function, 16  
point spread function, 14, 16  
pulsar, 2  
PyKE, 14

quarter, 22, 27

radial velocity, 3, 4

radius, 27

solar system, 1, 3  
starspot, 7, 22

temperature, 28  
transit, 4, 5, 8, 10, 11, 25, 27